IOSR Journal of Agriculture and Veterinary Science (IOSR-JAVS)
e-ISSN: 2319-2380, p-ISSN: 2319-2372. Volume 16, Issue 3 Ser. I (March. 2023), PP 01-16
www.iosrjournals.org

Application of Hyperspectral Imaging Technology for Microbial Contamination Detection: A Review

Honggang Fang [a, b, c], Lianming Xia [a, b, c*], Yemin Guo [a, b, c], Xia Sun [a, b, c], DianbinSu[a, b, c], Jin Hua [a, b, c]

[a] *School of Agricultural Engineering and Food Science, Shandong University of Technology, No. 266 XincunXilu, Zibo, Shandong 255049, China*
[b] *Shandong Provincial Engineering Research Center of Vegetable Safety and Quality Traceability, No. 266 XincunXilu, Zibo, Shandong 255049, China*
[c] *Zibo City Key Laboratory of Agricultural Product Safety Traceability, No. 266 XincunXilu, Zibo, Shandong 255049, China*
**Corresponding author: Professor Lianming Xia*

Abstract:
Agricultural products rich in nutrients satisfy human needs but also provide a good breeding ground for microbial growth. Every year microbial contamination of agricultural products causes serious economic losses and poses a serious threat to human and animal health. Due to the short timeframe of agricultural products it was particularly important to detect microbial contamination in a timely manner. Hyperspectral imaging (HSI) had become a current research hotspot in the field of non-destructive testing of agricultural products, as it can meet the needs for timely and high volume detection of microorganisms. This was because it combines the advantages of traditional imaging and spectroscopic techniques for non-destructive detection of the internal and external quality of agricultural products. This paper reviews the applications of HSI technology in the detection and analysis of microbial contamination of agricultural products in recent years, and demonstrates the feasibility of the technology in terms of spectral analysis, modelling methods, map fusion and detection accuracy for the qualitative, quantitative and spatial distribution detection of microorganisms. Based on the above summary, the challenges and prospects of the HSI technology-based detection technology for microbial contamination of agricultural products are presented.

Keywords: *Hyperspectral Imaging; Microbial; Detection; Agricultural products; Spectroscop*

Date of Submission: 02-03-2023 Date of Acceptance: 13-03-2023

I. Introduction

According to the World Health Organisation (WHO) more than 2.2 million people die each year worldwide from microbial diseases of food and water origin[1]. Agricultural products in the production process provide the conditions for microbial growth. In addition, climatic conditions such as high temperatures, high humidity and rainfall during food production can accelerate microbial growth leading to the breakdown of organic matter in agricultural products leading to mould and spoilage[2, 3]. Some microorganisms produce biologically active and toxic secondary metabolites which are a major hazard to humans[4]. In everyday life mycotoxins accompany agricultural products into the human body posing a great threat to human life and health. These toxins include aflatoxins, ochratoxins and fusarium toxins (DON)[5]. Aflatoxins are mainly produced by Aspergillus flavus and Aspergillus parasiticus and other toxic metabolites.

Aflatoxin B1 is the most toxic and has been designated as a major carcinogenic compound by the International Agency for Research on Cancer (IARC) of the World Health Organization (WHO) [6, 7]. Ochratoxin (OTA) causes damage to human organs it is still being studied for its carcinogenic effects on humans[8]. Fusarium ochratoxin (DON) is a tertiary carcinogen when consumed by people it can cause toxic reactions such as vomiting and diarrhea [2]. Every year the agricultural economy suffers huge losses due to microorganisms.

The current methods for detecting microorganisms and their metabolites are mainly chemical analysis methods [9], commonly used detection methods include culture methods [10], immunological detection methods [11, 12], molecular biology determination methods etc[13]. Their disadvantages are the need to destroy agricultural products, time-consuming and laborious, high professional level of detectors, and introduction of dangerous chemical reagents, poor repeatability of test results [13, 14].These methods cannot meet the requirements of modern agricultural products scale fast detection, how to quickly, real-time, on-site detection of

microbial contamination in agricultural products has become an urgent technical problem. The non-destructive detection methods of agricultural products infected with microorganisms include machine vision technology, which imitates the principle of human vision, but it is difficult to detect early mold in agricultural products[15].NIR-spectroscopy can detect the degree of mold pollution in agricultural products[16],and monitor the overall quality of agricultural products, which causes misjudgment of individual agricultural products with better quality [17].

HSI technology combines machine vision technology and NIR-spectroscopy [18] to simultaneously acquire spatial information and spectral information of each image element of the inspected object [19]. HSI technology can adequately detect both the organic composition of agricultural products and their internal quality, as well as the corresponding spatial distribution. In recent years, HSI technology has a certain research base in the detection of mold in agricultural products, and this paper summarizes and introduces the progress of HSI technology in microbial detection. The challenges and prospects of HSI technology-based detection of mold contamination of agricultural products based on previous studies are presented to further provide insights for the exploration of HSI technology application development.

II. Hyperspectral Imaging Technology

The concept of HSI technology was first proposed by Goetz[20].The spectral resolution of HSI technology is at the nanometer level, and it provides two wavelength ranges: 380-780 nm for the visible region and 780-2500 nm for the near-infrared region [21].The HSI technique can generate images of samples in different adjacent wavelength bands (generally less than 10 nm), and the resulting images are stacked by wavelength to form a hypercube (X, Y, λ) image [22]. λ-axis represents the wavelength and shows the spectral dimensional information, while X-axis and Y-axis show the spatial dimensional information, which form a three-dimensional data set, as shown in Fig 1.

A complete HSI system has a light source, imaging spectrometer, optical camera (surface array CDD detector), lens, mobile sample stage, computer image acquisition system and motion control system, etc. The system composition is shown inFig 2.

There are three modes of hyperspectral image acquisition, as shown in Fig 3, point-by-point scanning type, line push scanning type, and area scanning method [23]. The line-push scanning type is the most commonly used method for acquiring hyperspectral images in the detection of contaminated microorganisms in agricultural products, which has the characteristics of one-way continuous information acquisition to ensure information integrity, and in the process of line-push scanning, a single wavelength sample image is acquired each time, and all wavelengths are repeatedly acquired to form a hyperspectral image, also known as a data cube. Can be used for large-scale real-time detection of agricultural products.

Before acquiring a sample hyperspectral image, the camera dark current effect needs to be corrected to obtain a relative reflectance image I. The raw hyperspectral image needs to be calibrated as an absorbance image or reflectance image in order to analyze the image in the next step. The white reference image is acquired by using a 100% tetrafluoroethylene standard white plate (99% reflectance) for black and white calibration and the lens cap is placed over the lens (0 reflectance) to acquire the reference image in the dark.Equation (1) for calibrating the reflectance image of the original hyperspectral image is shown below.

$$I = \frac{I_{RAW} - I_D}{I_W - I_D} \times 100 \quad (1)$$

where $I$is a calibrated hyperspectral image, I_{RAW} is an original hyperspectral image, I_W is a white reference image; and I_D is a dark reference image.

III. Data Analysis

Hyperspectral images have a large amount of redundant information in the spatial and spectral domains.If all the information is used in the detection of agricultural products, it only increases the workload of processing data and does not reflect the advantages of hyperspectral technology better.After acquiring the image, the image needs to be further processed to obtain a robust model with strong detection capability.

3.1 Sensitive Region Spectral

The purpose of spectral image preprocessing is to eliminate the influence of non-uniform illumination, suppress pixel noise, remove relevant areas, and remove redundant information as much as possible. Pure perceptual region images (ROI) are obtained to improve data processing efficiency. Hyperspectral images with spectral data consist of a cube, and materials with different chemical composition and physical structure often exhibit different spectral characteristics and become spectral fingerprints. So the spectral fingerprint features of each pixel in the image can be used to detect and identify different objects, so the choice of threshold segmentation using images of different wavelength bands enable ROI extraction of different targets [24].

Principal component analysis (PCA) is one of the methods to extract perceptual region (ROI) by transforming variables through orthogonal transformation operation. Through orthogonal transformation, a set of multivariate data, matrix is transformed into a set of linearly uncorrelated variables in new coordinates, and the transformed variables are called principal components[25], and the score matrix of principal components is calculated by equation (2).

$T = XP + E$ (2);

Where T is a score matrix, $P$is a load matrix, and E is a spectral residual matrix. The combination of a principal component score map and a two-dimensional scatter plot allows the principal component score of each pixel to be associated with its position in the hyperspectral image, and a method for extracting regions of interest using interaction analysis of images and spectra.

3.2 Spectral Preprocessing

Hyperspectral technology in the process of agricultural products detection, the effect of spectral data from hyperspectral images does not meet the requirements of model building due to the influence of noise and light scattering. With the rapid development of computer technology, more and more spectral pre-processing methods have been generated.Spectral conversion is the conversion of a spectrum to absorbance 3 and Kubelka-Monk transform 4 is an effective way to reduce the nonlinearity of reflectance measurements, where the transmittance of a material sample is related to its absorbance according to the Beer-Lambert law [26].Thus reflectance measurements are similar to optical density readings and the differences can be amplified by spectral conversion.

$A = log_{10}（1/R）$(3)

$KM = (1 - R^2)/2R$(4)

Smoothing is a method of suppressing random noise caused by environmental differences, instrument stability, etc., and is used to obtain smooth and accurate spectral data.Smoothing methods include moving average method, Savvitzky-Golay, Gaussian and median filtering[27, 28].In the smoothing process, a window of a certain width is set, and "averaging" and "fitting" operations are performed for each point within this window.In the smoothing process, a window of a certain width is set, within which the "averaging" and "fitting" operations are performed for each point. Therefore, in order to obtain the best estimate of the points, it is necessary to set a suitable width of the smoothing window [29].

Standardization is a pre-processing method for a set of spectra based on a spectral array that can eliminate errors caused by light range differences, scattering, and sample dilution.The same preprocessing methods as the normalized attributes are variable normalization and multiple scattering correction [30].These two methods have similarities and have relatively high correction power compared to the multivariate scattering correction algorithm variable normalization.

Detrending algorithm is an effective method to eliminate the baseline of a diffuse reflectance spectrum. The spectral curve will be baseline shifted during the spectral acquisition. The detrending algorithm fit a trend line in the reference spectrum with a polynomial and then subtract this trend line from all the acquired spectral curves separately to obtain the detrended spectrum [31].This method removes the background information and amplifies the information of the sample itself [30]. Generally detrending algorithms and variable normalization algorithms are used in combination, with the trending algorithm performed first, followed by the variable normalization algorithm.

Derivative algorithm (Derivative) can better purify the spectrum information, effectively remove the background interference and baseline drift, play a role in splitting the peak, emphasize the small peak in the strong absorption, clear mechanism absorption wavelength [32].Sometimes, the noise is also emphasized and pseudo-harmonic peaks appear, so the need for differential processing needs to be determined according to the actual situation. In order to eliminate the noise brought by the spectral transformation and avoid emphasizing the noisy information, original spectrum is usually smoothed before derivation.Equations (5) and (6) represent the spectra of the discrete spectrum x at wavelength$k$ after performing the first-order and second-order derivatives of differential width g.

$x_{k,1s1} = \frac{x_{k+g} - x_{k-g}}{g}$(5)

$x_{k,2nd} = \frac{x_{k+g} - 2x_k + x_{k-g}}{g^2}$ (6)

3.3 Feature Wavelength Selection

Redundant information exists in the full wavelength, which also interferes with the information of the sample itself. Selecting the most effective spectral information from the whole wavelength can reduce the computational load and improve the computational efficiency [33]. Extraction of the optimal wavelength allows qualitative and quantitative studies with less error. Extraction of the characteristic wavelength requires the selection of a suitable method according to the actual situation including correlation coefficient method [33],

continuous projection algorithm [34], positive adaptive weighting method [35], genetic algorithm [36], regression coefficient method [37] and random frog algorithm [38]. Due to the complexity of hyperspectral data, several methods are usually used to select the characteristic wavelength for comparison, so as to provide the best characteristic wavelength for model establishment.

3.4 Modeling and Evaluation

Hyperspectral image information has the characteristics of high dimension and multi-collinearity, so it is necessary to use multivariate analysis method to establish the relationship between spectral information and sample reference value [39]. Generally, multivariate analysis includes quantitative analysis and qualitative classification.

In the process of qualitative analysis, classification methods are divided into unsupervised classification and supervised classification. Unsupervised classification divides data sets in samples that are not known in advance into different clusters, and conclusions can be drawn only after unsupervised classification is performed. However, supervised classification is based on an existing dataset and is trained to find associations between features and labels. Common supervised classification methods for spectral data include linear regression [40], k-nearest neighbor (KNN) [41], plain Bayes [42], support vector machines [43], decision trees [44], artificial neural networks [45] and partial least squares discriminant analysis [46]. Unsupervised classification has K-mean algorithm, self-encoder, and principal component analysis methods. Researchers usually evaluate the accuracy of qualitative classification models in the same way as overall accuracy, specificity, and sensitivity [47].

Quantitative analysis is performed to establish a link between the mapping data and the sample attributes, using both linear and nonlinear approaches to build models for detecting and predicting the sample attributes. The linear analysis methods are partial least squares regression analysis, principal component regression analysis, and multiple linear regression analysis. The nonlinear analysis methods are artificial neural networks and support vector machines. Quantitative analysis evaluates the model with the following metrics: coefficient of determination (R^2), root mean square error (*RMSE*) and residual prediction deviation (RPD) [48].

4. Application of HSI Technology in Microbiological Detection

With the development of HIS technology, the requirements for microbial detection in agricultural products have increased, and rapid and accurate detection of microbial contamination can reduce economic losses and unnecessary transition inputs of hazardous chemicals, which are of great significance in the quality testing of agricultural products. Table 1 shows the application of HIS technology to the detection of fungi, mycotoxins, bacteria and viruses. The development of HSI technology applied to microbial detection can be seen, and the following is the application of HIS technology in various microbial detection.

4.1 Application of HSI technology in fungal detection

Fungi can be found everywhere in our life, and there are many kinds of fungi, some of which are pathogenic and opportunistic fungi, invade human body and cause diseases. At the same time, the metabolites of some fungi, when consumed by humans, can produce some toxicity, such as carcinogenic, teratogenic, immunosuppressive, etc., which endanger human health and cause economic losses. The following are the HSI techniques used to detect major fungi and their metabolites in agricultural products.

4.1.1 Fusarium detection analysis

Crop infection with Fusarium(FHB) is also known as tombstone disease is a common disease of small grains such as wheat, oats and barley.The main causal agent of FHB is Fusarium graminearum Schwabe.Grain crops infected during the growing season may contain Fusarium secretions such as deoxynivalenol (DON), also known as vomitoxin.DON affects the quality of food and feed and endangers human health [49]. Therefore, HIS technology has been used to detect Fusarium graminearum Schwabe and DON.

The use of hyperspectral techniques for the detection of Fusarium has beendemonstrated in recent years. ***Williams et al***[25]inoculated three Fusarium species into potato dextrose agar for 55 h, 72 h, and 96 h of growth.Data acquisition was performed in the 1100-2498 nm range using HSI technology.PLS-DA and PCA methods were used for modeling. Although RMSEP best this results were only 0.39, 0.25 and 0.45 with R^2 of 0.999, 0.867 and 0.44. the results of the pixel analysis by PCA can be seen to have good results and clearly determine the three Fusarium properties.They also studied the growth characteristics of the three Fusarium species and constructed the growth characteristics of the most infantile, juvenile, young and old always classes of mycelium in colonies of the three Fusarium species in different time periods[25, 50][25, 50][25, 50][25, 50][25, 50][24, 49][23, 48][22, 47][21, 46][20, 45][19, 44][18, 43][17, 42][17, 4217, 42].***M. Nadimi et al*** used the NIR HSI technique to detect the presence of Fusarium and DON in wheat seeds using a K-nearest neighbor (KNN) classifier in the 960-1700 nm wavelength range [51].The results showed that the accuracy of Fusarium

infection in wheat seeds was 85% and the sensitivity was 92%, and the accuracy of fungal toxin deoxynivalenol (DON), a secondary metabolite of Fusarium contained in wheat seeds, was 80% and the sensitivity was 77% for the discrimination.The above study established that hyperspectral techniques can discriminate Fusarium.

As hyperspectral techniques allow for easy and rapid detection of Fusarium moreand more relevant studies are being developed. ***Muhammad A. Shahin*** used HSI technique in the range of 400-1,000 nm to qualitatively discriminate the degree of infestation in Fusarium oxysporum-infested seeds of red spring wheat in western Canada [52].A linear discriminant analysis (LDA) model was established by compressing the hyperspectral image data into 10 PCA scored images using the principal component analysis (PCA) method.The nuclei were classified into two stages: normal nuclei and damaged nuclei, and then the damaged nuclei were classified into mild nuclei and severe nuclei. Using LDA, intact and damaged nuclei could be classified with an overall accuracy of up to 92% and a prediction accuracy of up to 86% for the degree of Fusarium damage.The realization of hyperspectral techniques to discriminate the degree of Fusarium infestation of wheat seeds further provides HSI technology to provide a method for wheat screening.Data on wheat seeds and flour in the range of 400 - 1000 nm and 1,000-2,500 nm were investigated by ***Kun Liang et al*** [53].The preprocessing was performed by using two different methods of multiple scattering correction (MSC) and standard normal variables (SNV), effective wavelengths extracted by genetic algorithm (GA), support vector machine (SVM), sparse self-encoder (SAE) network for modeling quantitative classification. For the range of 400 – 1,000 nm MSC-GA-SAE model has the highest prediction accuracy (100% for both training and test sets). 1,000-2,500 nm range SNV-GA-SAE model has higher classification accuracy for shortwave infrared imaging data (100% for training set and 96% for test set). ***Rrpdc*** hyperspectral data acquisition of Fusarium yellows and Fusarium graminearum infected maize kernels was performed in the range of 1,000-2,500 nm [54]. The pre-processed data method used standard normal variation (SNV), first order derivative and SNV+ first order derivative to perform dimensionality reduction of the data using principal component analysis (PCA), and pixel-based PLS-DA model to classify Fusarium samples in the test set with 99.7% classification accuracy.***Guang hui Shen*** classified wheat seeds infected with DON into three classes (severely damaged, moderately damaged, and asymptomatically damaged) [49]. Support vector machine (SVM) and local PLS (LPLS-S) algorithm based on global PLS score were developed, and a quantitative model of DON was established by using HSI technology and HIGH performance liquid chromatography to analyze and verify DON content. LPLS-S method had the best simulation effect on seeds, with RMSEP of 40.25 mg/kg and RPD of 2.24. The degree of fusarium infection in wheat seeds was determined by detecting DON content.

The above illustrates that the discrimination of Fusarium by HSI technique can be achieved and provides a new method for further study of Fusarium. It provides a basis for future large-scale batch screening of wheat.

4.1.2 Analysis of aflatoxin detection

As one of the most harmful mold species in life, there are few studies on the detection of aflatoxin using HSI technology, including the detection of its metabolite aflatoxin. There are also many articles on the use of HSI to detect Aspergillus flavus and its metabolites.It can be seen that with the development of information technology, HSI detection of aflatoxin is slowly moving towards industrial grade applications.

Jin et al [55]explored the feasibility of using the V-NIR (400-1000 nm) HSI system to discriminate whether different aflatoxins were produced under the same conditions.The images acquired under different light sources were discriminated to derive qualitative discrimination between (AF38, AF283) under halogen light sources and (AF13, AF38) under UV light sources.The classification results under halogen light source were compared with those under UV light source, and the classification accuracy under UV light was higher.It is noteworthy that the pixel-level classification accuracy for (AF38, AF283) and (AF13, AF38) under UV light source was above 95% on average. This result can prove that Aspergillus flavus can be differentiated between categories in HSI technique, obtaining better diffuse reflectance of Aspergillus flavus as well as aflatoxin under violet light source.***Kandpal et al***[56]. reported a study applying the HSI technique short-wave NIR (1100-1700 nm) for the detection of maize seeds of three varieties whose surfaces were contaminated by four concentrations of AFB1 (10, 100, 500, and 1000 mg\kg) in dilution.A classification model was developed using PLS-DA to identify maize kernels with different levels of contamination.The final results for the three maize varieties, white, purple and yellow, were 92.3%, 96.9%, and 90.7%, respectively.The beta coefficients of the PLS-DA model were applied to each pixel point of the hyperspectral image to finally generate an AFB1 distribution map for each contaminated maize kernel, achieving the visualization of AFB1-infested maize kernels that could not be achieved by traditional techniques, and providing accurate spatial location information for maize infected with aflatoxin.

Daniel Kimuli et al [57]explored the feasibility of using a 400-1000 nm HSI system to detect AFB1 on the surface of maize. There were four different yellow maize varieties, and four different concentrations (10, 20, 100 and 500 ppb) of AFB1 dilutions were applied manually on the surface of the maize kernels of each variety, using a methanol solution as a reference object for the application. For data analysis, the PCA method was

applied to reduce the dimensionality of the HSI data, and then the PC variables generated by PCA were analyzed using FDA. Finally, an identification accuracy of 98% was achieved for all samples pooled from four maize varieties, while discriminant analysis was performed on maize seeds coated with different concentrations. This result fully demonstrates the feasibility of using the VNI- HSI system to detect the presence of AFB1 on the surface of maize seeds. In a subsequent study, the 1000-2500 nm HSI system was used to detect AFB1 on the surface of maize seeds[57]. Treatment and last treatment method in addition to the PLS-DA method was used. Combining standard normal variables and first-order derivative pretreatment, the results of the classification tests performed on different varieties were erratic, with high classification accuracy for individual varieties. The calibration and validation accuracies of the PLS-DA classification model for Illinois varieties were 100% and 96%. The poorer aflatoxin classification results of the PLS-DA and FDA models for mixed samples were due to the limited variation in the chemical composition of the mixed samples as the PLS-DA and FDA models may have received less information about the use of AFB1 to separate the mixed samples. The large difference in AFB1 detection accuracy between the two studies may be due to the different spectral absorption of maize components in V-NIR and S-WIR. In general, moisture and fat are more sensitive to spectra in the S-WIR range. Therefore, the SWIR band absorbs moisture and fat more strongly than the VNIR band. This is the fundamental reason for this difference

With the newer development of data processing methods, ***Feifei Tao et al*** used hyperspectral techniques to identify aflatoxin infection in maize seeds using new data processing methods[58].NIR HSI in the 900-2,500 nm spectral range was investigated to identify kernels inoculated with Aspergillus flavus (AF13) and kernels inoculated with non-Aspergillus flavus (AF36). The classification rate of non-aflatoxigenic and aflatoxigenic kernels was 97.8% using partial least squares discriminant analysis (PLS-DA) method based on full average spectra of 3 levels of control extracted from the same kernel side. Using different kernel-side full-average spectra, the highest average overall prediction accuracies of 91.5% and 95.1% were obtained for class 3 and class 2 models. Using the most important 30, 55, and 100 variables identified by the random frog (RF) algorithm, the simplified I-RF-PLSDA model had average overall prediction accuracies of 87.7%, 93.8%, and 95.2% for both types of discriminations using different kernel-side information. The average overall prediction accuracy of the II-RF-PLSDA model using these 25 variables and 75 variables over 100 random runs was 82.3% and 94.9%. It can be seen that the more variables there are, the correspondingly higher the accuracy of the model, which is advantageous when applied to detect large amounts of maize.

Han Zhong zhi[59] dropped different concentrations of aflatoxin solutions (10ug/L, 20ug/L, 50ug/L, 100ug/L, 10mg /L) on peanut kernels by HSI system in the range of 400-1000nm.Hyperspectral images in 33 bands (400 -720 nm) were then acquired for each sample using the HSI system under 365 nm ultraviolet (UV) light.Four fluorescence indices are proposed, namely, radiation index (RI), difference radiation index (DRI), ratio radiation index (RRI) and normalized difference radiation index (NDRI).Finally, narrow-band spectra were obtained by optimization of Fisher's method, and aflatoxin was identified using RBF-SVM model and regression analysis was performed on the degree of aflatoxin contamination.The experimental results show that the accuracy of the 5-fold cross-validation of the support vector machine is 95.5%, and the mean square error (MSE) and correlation coefficient are 0.0223 and 0.9785, respectively.The above findings have positive implications for the online detection and classification of aflatoxins in agricultural products.***Gao***[60] in the same lab used a one-dimensional convolutional neural network model to investigate the presence of aflatoxin in a pixel on a hyperspectral image.Simultaneous detection of corn and peanut, in training on both grain data, yielded the highest result of 92.11% for corn detection accuracy and 96.35% for peanut detection accuracy. Mixing the two types of data together for training produced the highest accuracy result of 94.64%. In terms of feature selection, the highest detection accuracies for peanut, corn, and mixed data were 85.48%, 79.70%, and 83.96%. The above two studies provide the basis for future real-time testing of agricultural products at scale.

Quan Zhou et al [61] obtained hyperspectral images at 430-1000 nm and long-wave NIR 1,000-2,400 nm. Three concentrations (10, 20 and 30 ppb) of AFB1 were applied to the study maize seeds and a set of controls, and the raw data were preprocessed using Savitzky-Golay (SG) smoothing, multiplicative scattering correction (MSC) and first-order derivative (FD) methods. The between-class variance rate (BWVR) and weighted between-class variance rate (WBWVR) were used for the selection of feature wavelengths, and three models of support vector machine (SVM), K-nearest neighbor (KNN), and decision tree (DT) were developed for comparison. The accuracy of the SVM model built under 10 feature wavelengths selected by the WBWVR method was as high as 96.18%, verifying the effectiveness of BWVR and WBWVR in the selection of feature wavelengths. This study provides a new approach for the selection of characteristic wavelengths.***Gayatri Mishra***studied single grain almonds infected with AFB1 by hyperspectral techniques in the 900-1,700 nm range [62], using PLSR modeling combined with appropriate spectral preprocessing techniques, withR^2 of 0.958 and RMSEP of 0.089 µg/g for the curvilinear regression model by competitive adaptive reweighted sampling CARS method for feature wavelength selection by multiple linear regression (MLR) modeling showed R^2 of 0.948 and RMSEP of 0.090 µg/g for the characteristic wavelengths.

In the above application of HSI technology for aflatoxin detection of Aspergillus and its different categories of aflatoxin found that for aflatoxin has a fluorescent effect under the violet light, which is conducive to improving the discrimination accuracy, in the future HSI system design can increase the design of light source types to enhance the ability of HSI technology in nondestructive test.

4.1.3 Analysis of anthrax detection

Anthracnose is particularly harmful to crops. Infection by a fungus causes leaf and fruit rot of crops, which seriously threatens the quality and yield of cash crops. The application of HSI technology in anthrax detection is described below.

Chu Xuanstudied the growth characteristics of two anthrax bacteria (colletotrichumtruncatum, colletotrichumgloeosporioides) using visible near-infrared (380-900 nm) HSI technology [63]. The SVM model developed using these wavelengths was able to identify the growth days of anthrax with an accuracy of 97.50%. The results showed that NIR HSI was effective in evaluating the growth characteristics of colletotrichumtruncatum and colletotrichumgloeosporioides, which is the first study to cause plant anthracnose. ***Yuan*** used the HSI technique in the visible range for tea tree anthracnose detection [64]. Disease sensitivity bands at 542, 686 and 754 nm were identified by spectral sensitivity analysis, and two new disease indices were established using these bands: the Tea Anthacnose Ratio Index (TARI) and the Tea Anthacnose Normalization Index (TANI). A crust detection method combining unsupervised classification and adaptive two-dimensional thresholding is proposed, which is independent of leaf background differences compared with traditional pixel-based classification methods and provides an effective means for disease identification and disease analysis. The validation results showed that the overall disease identification accuracy was 98% and 94% at the leaf level and pixel level, respectively. The above study showed that it is feasible to achieve automatic and accurate detection of tea anthracnose using HSI technology.

Fazari used a visible HSI system to discriminate olives that had been inoculated with anthrax using a deep convolutional neural network to evaluate his model in terms of accuracy, sensitivity and specificity, with sensitivity being the fraction of infected olives detected and specificity being the fraction of healthy olives correctly identified [65].The results show an accuracy of only 80% (due to 80% of infected samples), a specificity of 0 (healthy olives will never be identified) and a sensitivity of 100% (all infected olives will be detected), and with the extension of the inoculation time after the fifth day the identification of anthrax infection in olives can reach 100% accuracy. Further optimization of the model is needed relative to the specificity data, and this is a further study for future deep convolutional neural network models for Bacillus anthracis detection.***Yu-Hui Yeh*** studied strawberry leaves infected with anthrax by acquiring images of strawberry leaves inoculated with the anthrax fungus at three infection stages (healthy, latent and symptom onset) in an HSI system in the wavelength range of 400-960 nm[66]. Spectral angle mapping (SAM), stepwise discriminant analysis (SDA) and self-learning correlation measure (CM) methods were used blindly to study the three different infection stages. The accuracy of the classification results for the three infection stages was about 80%. For two infection stages (healthy and symptomatic), the average accuracy was as high as 80%. The classification accuracy for the three infection stages was approximately 80%. For two infection stages (healthy and symptomatic), the average accuracy was as high as 80%. In fact, the average accuracy of the two-stage SDA classification was 93%. Therefore, the use of HSI technique to detect foliar anthrax infected areas is more practical and effective than the traditional destruction methods.

For the prevention of anthrax is not only detection, we have to carry out prevention, and the detection using HSI technology becomes more important during the incubation period of anthrax infection in agricultural products. In the above study, the identification of different anthrax species reached an accuracy rate, as well as the identification of agricultural products infected with different levels of anthrax. Therefore, accurate and rapid identification can be achieved in future plant protection and fruit screening using HSI technology.

4.1.4 Other Fungal Mycorrhizal Detection Analysis

Yao Lu studied five common cereal fungi Aspergillus parasiticus (Aspergillus parasiticus), Aspergillus flavus (Aspergillus flavus), Aspergillus glaucus (Asper gillusglaucus), Aspergillus niger (Asper gillusniger) and Penicilliumsp by HSI technique [67].The SVM classification model is built after selecting the best wavelength by the successive projection algorithm (SPA).The results showed that the accuracy rate of Asper gillusniger and Penicilliumsp was above 95.87%. The average accuracy and Kappa coefficient of SPA-SVM method were 98.89% and 0.97 for HSI images of 5 fungi growing for one day. These results indicated that HSI technology could be used to evaluate the growth characteristics of cereal fungi, further indicating that HSI technology could be used to distinguish different fungi, and the classification accuracy could reach the industrial level.

T. Senthilkumar used hyperspectral techniques in the 1000 ~ 1600 nm range to detect the discrimination of rapeseed grains [68], barley [69] and wheat [70] infected with both fungi (Aspergillus glaucus and Penicillium spp), all using linear discriminant analysis (LDA), quadratic discriminant analysis (QDA) and

martinet classification modeling was performed. The three classifiers first classified healthy and infected rape seeds with an accuracy of more than 95%, and more than 90% at the beginning of infection with Aspergillus glaucus and Penicillium spp. The classification accuracy improved to 100% as the time of infection with the fungus increased. The detection and classification of different grains by the three models was achieved, which can save a lot of algorithm application for future application to practical production.

Jessica Farrugia examined mold in cheese using the HSI technique in the 400-1000 nm range [71], using the PCA method to locate early mold in cheese after scoring the hyperspectral images in the visible portion, for agar and cheese, the first three principal components can contain more than 99% of the total variance, using the second principal component projection to highlight mold on cheese that is true for the presence of contaminants on the test samples. Although the mold on the cheese could be detected by map fusion, no distinction was made to distinguish the mold category and content. ***Sholeem Griffin*** from the same laboratory developed a sterile cheese model to study the potential of HSI technology for fungal detection [72]. The model cheese was challenged with S. aureus to create an untrained PCA model that could be used to compare the cheese model after colony formation to determine a generalized cheese model for fungal contaminant assessment by HSI technology. The above two methods allow the application of the HSI technique to the detection of early colonization of solids and semi-solids of dairy products in industry, and can be extended to industrial-scale testing of other agricultural products.

Sun Yedemonstrated the fungal growth characteristics of gray mold, rhizobia and conidia using HSI technique in the range of 400-1000 nm [73]. Qualitative analysis was performed in the time range, and it was concluded that the three fungi were most easily distinguished at 36 h with an accuracy of 97.5%, and the R^2 of the growth simulation models for the three fungi in the training and validation sets were 0.9292, 0.9927, 0.7832 and 0.8594, respectively. The study had a single variable for inoculation on the medium, and the environment for complex samples in actual production further research is needed.

Hongzhe Jiang team investigated the detection of oleaginous fruit mold in natural environment using HSI technique in the visible light (400-1000 nm) range [74]. The best modeling method was PLS-DA with an accuracy of 90.8%, and the three modeling methods were PLS-DA, KNN and CART. The model was simplified by selecting the feature wavelengths through competitive adaptive reweighted sampling algorithm (CARS), and the correct classification rate of 83.3% was obtained for the prediction set of CARS-PLS-DA model. Minor, moderate and severe mold can be effectively distinguished by principal component analysis combined with visualization studies.

Yan-Ru Zhao et al. used NIR-hyperspectral techniques to obtain images of rape petals (874-1,734 nm) to detect infection with Sclerotinia sclerotiorum[75]. The characteristic wavelengths were selected using two methods, PCA and RF, and the optimal model was established based on the full and optimal wavelengths using the LS-SVM method, and finally the model was evaluated using the area under the subject's working characteristic curve (AUC).The model classification is correct at 100% under the full band and the highest model accuracy of 97.48% is established by the XSL-LS-SVM method under the optimal band. The model evaluation is 1 under the full band and 0.929 under the optimal band. How to improve the classification accuracy by modeling in the optimal waveband is the key to the future application of hyperspectral technology for large-scale detection.

4.2 Application of HSI Technology in Bacterial Detection

Bacterial diseases cause agricultural decay, endanger food safety and have an impact on future agricultural development, while bacteria are more harmful directly to humans.There are still relatively few applications of hyperspectral techniques for the detection of bacteria, and the following is a description of the rapid nondestructive detection of bacteria by HSI techniques.

The potential of multivariate data analysis as a rapid non-destructive tool for bacterial detection and differentiation was investigated by ***Williams et al.*** using NIR HSI in the range of 920-2,514 nm for Bacillus, Escherichia coli, Salmonella enterica, Staphylococcus aureus and Staphylococcus epidermidis[76]. Mean central data were analyzed using PCA. Standard normal variables (SNV) correction and Savitzky-Golay technique (second order derivative, third order polynomial; 25-point smoothing) were used. The correct rate of distinguishing different bacteria in both PCA scoring plots in the PC1 and PC2 directions was less than 50%, and the rate of distinguishing B. cereus from Escherichia coli and Streptococcus enteritidis in the PC1 direction was 59%, and in the PC2 direction was 6.85%. The separation of Staphylococcus epidermidis from Bacillus cereus and Staphylococcus aureus along the PC1 (37.5%) direction was not very effective from an overall view, and the reason here is mainly that this is related to the difference in amino acid and carbohydrate content. A partial least squares discriminant analysis (PLS-DA) model was used to validate the PCA data. The best predictions were made for Bacillus cereus and Staphylococcus spp. and the correct percentage of predicted pixels ranged from 82.0 ~ 99.96%. But there is also the specificity reported if for a colony more than 50% of the pixels were identified as a particular bacterium using the pixelation method. To solve the above trouble, it is also

necessary to combine pixel and spectral information to improve the prediction accuracy.

Lin Huang studied the total viable count (TVC) in pork by acquiring hyperspectral images at 450-900 nm, selecting 100 feature variables using the PLS method and image variables by the PCA method, and modeling them using the back propagation artificial neural network (BP-ANN) method [77]. The model based on data fusion outperformed other models with prediction set RMSEP = 0.243 lg CFU/g, R_P^2 = 0.8308. ***Feng*** also used hyperspectral techniques for the detection of TVC in chicken breast, and both studies used different modeling approaches but combined graphical fusion to improve the prediction set model while visualizing the exact location of TVC [78]. The combination of map fusion techniques is an important direction for the future use of hyperspectral techniques for microbial detection in agricultural products.

Danrui Liexplored the potential of the HSI technique to measure surface contamination of freshly cut potato slices in the visible-near infrared (Vis-NIR, 400-1000 nm) region [79]. Four preprocessing methods (first-order derivative (F-D), second-order derivative (S-D), multiplicative scattering correction (MSC), standard normalized variables (SNV)) and their combinations were investigated, and linear and nonlinear regression models were developed using genetic algorithms for the processing of spectral data and the selection of characteristic wavelengths. The prediction accuracy of the full-spectrum-based backward-passage neural network (BP-NN) model was 97.6%, and the residual prediction deviation (RPD) was 6.7. In this study, a non-thermal environment-friendly method was successfully explored for the optimal inactivation time (20 min) of Escherichia coli on the surface of fresh-cut potato slices, and the overall results showed that HSI can provide rapid and nondestructive detection of foodborne pathogens on the surface of fresh-cut products. The overall results showed that HSI can provide a method for rapid and non-destructive detection of foodborne pathogens on the surface of fresh-cut products. The model built based on the full spectrum is computationally intensive and has potential stability problems.

Feifei Tao studied pork tenderness and E. coli contamination by HIS technique in the visible-near infrared (Vis-NIR, 400-1000 nm) range [80].The scattering profile was fitted using the Lorentz distribution function to obtain three parameters a (asymptote), b (peak) and c (full width at b/2).The results showed that the correlation coefficients of the MLR models using parameters a, b, (b-a) and (b-a)/c to predict pork tenderness were 0.831, 0.860, 0.856 and 0.930, respectively.For E. coli-contaminated pork, the RCVs of the MLR models based on parameters a and a&b&c were 0.877 and 0.841, respectively.The overall study showed that the spatially resolved hyperspectral scattering technique combined with multiple linear regression was able to predict pork tenderness and E. coli contamination.***Yao-Ze Feng et al*** used HSI in the visible-near infrared (Vis-NIR, 400-1000 nm) range to classify three strains of E. coli (i.e., E. coli O8, O11 and O138), two strains of Listeria monocytogenes (i.e., L. monocytogens and L. seeligeri) and golden Staphylococci were subjected to rapid classification[81].After three chemometric methods (comparing genetic algorithm, particle swarm algorithm, and IWO algorithm) were optimized, the IOW algorithm was finally selected to be more effective.After building a simplified model by three methods of feature wavelength selection through competitive adaptive reweighted sampling (CARS), genetic algorithm (GA) and successive projection method (SPA), the effect is the best correction and prediction of the simplified IWO-SVM model with feature wavelengths selected by CARS is 97.2% and 96% respectively.This study realizes that the HSI technique holds great promise for the classification of bacteria at the subspecies level.

Ernest Bonah used visible near infrared (Vis-NIR, 400-1,000 nm) HSI technique to study (Escherichia coli ATCC 25922, Escherichia coli O157: H7 ATCC 35150, ampicillin-resistant Escherichia coli, Listeria monocytogenes ATCC 19115, Staphylococcus aureus ATCC 25923, (Methicillin-resistant Staphylococcus aureus T34, Salmonella enterica CICC 21482, Salmonella typhimurium CICC 22956) are the best models for the classification and discrimination of eight bacteria[82]. After comparing the results the final CARS-PSO-SVM model was established with the highest accuracy of 99.47% and 98.44% in training and prediction, respectively.In the same year he used visible near infrared (400-1,000 nm) HSI technique and partial least squares regression algorithm (PLSR) for rapid monitoring of foodborne pathogenic bacteria (E. coli O157 and S. aureus) contamination in fresh pork [82].The full band was then selected for characteristic wavelengths using population analysis (MPA), intelligent optimization algorithm and mixed variable optimization algorithm, and the VCPA-GA algorithm had the highest RPD for E. coli (R_p^2 = 0.9977; RMSEP = 0.1532; RPD = 13.5910), S. aureus (R_p^2 = 0.9960; RMSEP = 0.1225; RPD = 16.8032).This study is quite promise in model, make full use of the advantages of hybrid strategy use a smaller optimization variable space advantageous algorithm to improve the accuracy of the model, while the location of bacteria can be located, take full advantage of the fusion with the map, for the next HSI technology in the food industry for real-time monitor of bacterial control and inactivation mechanism.

4.3 Application of HSI technology in virus detection

HSI technology for the detection of viruses is relatively little research, but viruses produce significant harm to agricultural products as well as human life and health, the following is my literature from recent years to identify the HSI technology to detect viruses related reports.

Qing Gu et al. used HSI technique in the range of 400-1000 nm for tomato wilt virus detection [83]. Three feature wavelength selection methods were used to select 128 feature wavelengths, with continuous projection method (SPA), enhanced regression tree (BRT) and genetic algorithm (GA).The 128 bands were analyzed by machine learning algorithms (ML) including Augmented Regression Trees (BRT), Support Vector Machines (SVM), Random Distribution Forests (RF) and Categorical Regression Trees (CART).The results show that the best results can be obtained with an average overall accuracy of 85.2% and an area under the receiver operating curve of 0.932 using the characteristic wavelength selected by SPA as the input quantity and the BRT algorithm as the model.The results of band selection and variable contribution analysis of BRT modeling indicated that the NIR spectral region is informative and significant for the identification of tobacco infested and healthy leaves.

Hoonsoo Lee classified cucumber green spot mosaic virus (CGMMV)-infested watermelon seeds [84]. The classification results indicated that the HIS technique could be applied to the watermelon residual seed screening technique.Sarah L. MacDonald also tested for grapevine leafroll virus 3 (glav-3) in grape farms.Drones combined with HSI technology can provide accurate monitoring and prediction of vineyards in natural environments. This research moves from the laboratory to practical application scenarios, providing a further development of HSI technology applied to agricultural production.

IV. Conclusion And Future Trends

This paper reviews the application of HSI technology for microbial detection and concludes that HSI technology can have great potential for microbial detection.However, a large number of studies have been conducted on assays in a single setting.The natural environment in which agricultural products exist is complex and variable, and the types of microorganisms they contain are beyond human control, making it more difficult to monitor early infection of agricultural products with microorganisms.The above reported qualitative and quantitative testing of fungal contaminated agricultural products can achieve detection accuracy of more than 90%, and the accuracy of mycotoxin detection is between 80% and 100%.The reason for this difference is that the fungus damages the agricultural products and changes the physical and chemical properties of the agricultural products during the growth process.However, agricultural products contaminated only with metabolites of microorganisms have relatively little change in their own physicochemical properties.In addition, the use of HSI technology to detect some metabolites in cereals such as aflatoxin content and other national standards are very low, it is difficult to achieve high precision quantitative detection, and the detection threshold can reach the upper limit of the law issued by the food safety section.

In response to the above limitations of HSI technology, and to future research trends. First, to make HSI technology more suitable for automatic industrial inspection, the cost of HSI instruments must be reduced.Therefore, the software and hardware of HSI systems should be further improved to develop more cost-effective HSI systems, develop convenient handheld, dependent on other equipment for different working environments, improve their compatibility, and further make HSI technology for the inspection market.Second, there is a large amount of redundant data in hyperspectral images, and it generally takes a long time to obtain hyperspectral data and select specific models in the face of detecting different substances.It has become an inevitable trend to develop an HSI system that can obtain spectral images of only a few characteristic wavelengths.The development of hyperspectral detection technology requires more hyperspectral hand-held instruments. From the simplest detection sample simplification to detection sample diversification, as well as functional diversification development, application in different places.Of course, it is also necessary to design optimal algorithms to enrich the variable selection methods.Finally, the hyperspectral data have severe multi-collinearity, resulting in poor stability performance of the proposed model and lack of convincing experimental results.In future research needs to be explored around the shortcomings faced, and research into efficient, robust and accurate detection models will be another new development trend. At the same time design specific HSI technology instruments to detect products, has achieved rapid and accurate detection purposes

Disclosure statement

All the authors declares that they have no conflict of interest.

Funding

This work was supported by the Shandong Provincial Science and Technology Achievement Transfer Subsidy (Lu-Yu Science and Technology Cooperation) LYXZ10, Zibo-Sdut Integration Development Project，2019ZBXC090

Ethical approval

This article does not contain any studies with human participants performed by any of the authors.

References

[1]. W.N. Gichohi-Wainaina, N. Kumwenda, R. Zulu, J. Munthali, P.J.F.C. Okori, Aflatoxin contamination: Knowledge disparities among agriculture extension officers, frontline health workers and small holder farming households in Malawi, 121 (2021) 107672.
[2]. W. Awad, K. Ghareeb, J.T. Zentek, The Toxicological Impacts of the Fusarium Mycotoxin, Deoxynivalenol, in Poultry Flocks with Special Reference to Immunotoxicity, 5 (2013).
[3]. A. Ja, B. Gv, B. Gm, B. Slt, Fungal contamination and aflatoxin content of maize, moringa and peanut foods from rural subsistence farms in South Haiti - ScienceDirect, 85.
[4]. M.J.T. Buszewska-Forajta, Mycotoxins, invisible danger of feedstuff with toxic effect on animals, 182 (2020) 34-53.
[5]. Wang, D. Sun, J. Wen, FangTao, W. Ping, F. Cheng, R.J.C. Amp, F. Industry, Influences of corn oil production process on corn gibberellic ketene and vomiting toxins, (2015).
[6]. J.H. Ramirez-Prado, G.G. Moore, B.W. Horn, I.J.F.G. Carbone, Biology, Characterization and population analysis of the mating-type genes in Aspergillus flavus and Aspergillus parasiticus, 45 (2008) 1292-1299.
[7]. C.J.F. Ramos, C. Toxicology, Occurrence and exposure assessment of aflatoxins in Catalonia (Spain), (2013).
[8]. A. Pfohl‐Leszkowicz, R.A.J.M.N. Manderville, F. Research, Ochratoxin A: An overview on toxicity and carcinogenicity in animals and humans, 51 (2010).
[9]. A. Qtp, B. Nsl, The development of on-line surface defect detection system for jujubes based on hyperspectral images.
[10]. M.H. Brodsky, P. Entis, M.P. Entis, A.N. Sharpe, G.A.J.J.o.F.P. Jarvis, Determination of Aerobic Plate and Yeast and Mold Counts in Foods Using an Automated Hydrophobic Grid-Membrane Filter Technique, 45 (1982) 301-304.
[11]. A.L. Patey, S. Matthew, G.J.J.o.A.I. John, Determination of Total Aflatoxin Levels in Peanut Butter by Enzyme-Linked Immunosorbent Assay: Collaborative Study, (1992) 4.
[12]. P. Mukherjee, S. Ghosh, T. Ramamurthy, M.K. Bhattacharya, A.K.J.J.J.o.I.D. Mukhopadhyay, Evaluation of a rapid immunochromatographic dipstick kit for diagnosis of cholera emphasizes its outbreak utility, 63 (2010) 234-238.
[13]. K. Bjornsdottir-Butler, J.L. Jones, R. Benner, W.B.J.F.M. Iii, Development of a real-time PCR assay with an internal amplification control for detection of Gram-negative histamine-producing bacteria in fish, 28 (2011) 356-363.
[14]. M. Wiedmann, F.J.A. Barany, e. microbiology, Detection of Listeria monocytogenes with a nonisotopic polymerase chain reaction-coupled ligase chain reaction assay, 1993. 2743-2745=.
[15]. S.S. Harakannanavar, J.M. Rudagi, V.I. Puranikmath, A. Siddiqua, R. Pramodhini, Plant Leaf Disease Detection using Computer Vision and Machine Learning Algorithms, Global Transitions Proceedings, (2022).
[16]. C.D.J.旭. Sirisomboon, Early Detection of Ochratoxigenic Fungi on Green Coffee Beans by Near Infrared Spectroscopy, (2016).
[17]. F. Shen, T. Zhao, X. Jiang, X. Liu, Y. Fang, Q. Liu, Q. Hu, X.J.L.W.U.T. Liu, On-line detection of toxigenic fungal infection in wheat by visible/near infrared spectroscopy, 109 (2019) 216-224.
[18]. H. Kaya-Celiker, P.K. Mallikarjunan, A.J.F.C. Kaaya, Mid-infrared spectroscopy for discrimination and classification of Aspergillus spp. contamination in peanuts, 52 (2015) 103-111.
[19]. J. Chen, T. Bai, N. Zhang, L. Zhu, X. Zhang, Hyperspectral Detection of Sugar Content for Sugar-sweetened Apples Based on Sample Grouping and SPA Feature Selecting Methods, Infrared Physics & Technology, (2022) 104240.
[20]. P.H.J.I.J.o.P. Hsu, R. Sensing, Feature extraction of hyperspectral images using wavelet and matching pursuit - ScienceDirect, 62 (2007) 78-92.
[21]. B.C. Gao, M.J. Montes, C.O. Davis, A.J.R.S.o.E. Goetz, Atmospheric correction algorithms for hyperspectral remote sensing data of land and ocean, 113 (2009) S17-S24.
[22]. H.-J. He, D. Wu, D.-W. Sun, Potential of hyperspectral imaging combined with chemometric analysis for assessing and visualising tenderness distribution in raw farmed salmon fillets, Journal of Food Engineering, 126 (2014) 156-164.
[23]. J. Skvaril, K.G. Kyprianidis, E.J.A.S.R. Dahlquist, Applications of near-infrared spectroscopy (NIRS) in biomass energy conversion processes: A review, (2017).
[24]. G.M. Elmasry, S.J.B.E. Nakauchi, Image analysis operations applied to hyperspectral images for non-invasive sensing of food quality–A comprehensive review, 142 (2016) 53-82.
[25]. P.J. Williams, P. Geladi, T.J. Britz, M.J.A. Manley, b. chemistry, Near-infrared (NIR) hyperspectral imaging and multivariate image analysis to study growth characteristics and differences between species and strains of members of the genus Fusarium, 404 (2012) 1759-1769.
[26]. M. Wocher, K. Berger, M. Danner, W. Mauser, T. Hank, Hyperspectral Retrieval of Canopy Water Content Through Inversion of the Beer-Lambert Law, IEEE International Geoscience and Remote Sensing Symposium, 2018.
[27]. Y.R. Fan, T.Z.J.N. Huang, Hyperspectral image restoration via superpixel segmentation of smooth band, 455 (2021).
[28]. G. Li, S. Ma, K. Li, M. Zhou, L. Lin, Heterogeneity classification based on hyperspectral transmission imaging and multivariate data analysis, Infrared Physics & Technology, 123 (2022) 104180.
[29]. M. Beitollahi, S.A. Hosseini, Using Savitsky-Golay Smoothing Filter in Hyperspectral Data Compression by Curve Fitting, Electrical Engineering (ICEE), Iranian Conference on, 2018.
[30]. A. Femenias, F. Gatius, A.J. Ramos, V. Sanchis, S. Marín, Standardisation of near infrared hyperspectral imaging for quantification and classification of DON contaminated wheat samples, Food Control, 111 (2020) 107074.
[31]. A. de Cheveigné, D. Arzounian, Robust detrending, rereferencing, outlier detection, and inpainting for multichannel data, NeuroImage, 172 (2018) 903-912.
[32]. T. Wang, G. Li, C. Dai, Soluble Solids Content prediction for Korla fragrant pears using hyperspectral imaging and GsMIA, Infrared Physics & Technology, 123 (2022) 104119.
[33]. Q. Zhou, W. Huang, S. Fan, F. Zhao, D. Liang, X. Tian, Non-destructive discrimination of the variety of sweet maize seeds based on hyperspectral image coupled with wavelength selection algorithm, Infrared Physics & Technology, 109 (2020) 103418.
[34]. L. Pang, L. Wang, P. Yuan, L. Yan, J. Xiao, Rapid seed viability prediction of Sophora japonica by improved successive projection algorithm and hyperspectral imaging, Infrared Physics & Technology, 123 (2022) 104143.
[35]. H. Li, Y. Liang, Q. Xu, D. Cao, Key wavelengths screening using competitive adaptive reweighted sampling method for multivariate calibration, Analytica Chimica Acta, 648 (2009) 77-84.
[36]. K. Song, L. Li, L.P. Tedesco, S. Li, N.A. Clercin, B.E. Hall, Z. Li, K. Shi, Hyperspectral determination of eutrophication for a water supply source via genetic algorithm–partial least squares (GA–PLS) modeling, Science of The Total Environment, 426 (2012) 220-232.
[37]. D. Ashourloo, H. Aghighi, A.A. Matkan, M.R. Mobasheri, A.M.J.I.J.o.S.T.i.A.E.O. Rad, R. Sensing, An Investigation Into Machine

Learning Regression Techniques for the Leaf Rust Disease Detection Using Hyperspectral Measurement, 9 (2016) 1-8.
[38]. J. Chen, G. Li, Prediction of moisture content of wood using Modified Random Frog and Vis-NIR hyperspectral imaging, Infrared Physics & Technology, 105 (2020) 103225.
[39]. N.A. Aviara, J.T. Liberty, O.S. Olatunbosun, H.A. Shoyombo, S.K. Oyeniyi, Potential application of hyperspectral imaging in food grain quality inspection, evaluation and control during bulk storage, Journal of Agriculture and Food Research, 8 (2022) 100288.
[40]. C. Manis, C. Malegori, E. Alladio, M. Vincenti, P. Garofano, F. Barni, A. Berti, P. Oliveri, Non-destructive age estimation of biological fluid stains: An integrated analytical strategy based on near-infrared hyperspectral imaging and multivariate regression, Talanta, 245 (2022) 123472.
[41]. Y. Guo, S. Han, Y. Li, C. Zhang, Y. Bai, K-Nearest Neighbor combined with guided filter for hyperspectral image classification, Procedia Computer Science, 129 (2018) 159-165.
[42]. J.X. He, S.B. Chen, Y. Wang, Y.F.J.G.P. Wu, An Accurate Approach to Hyperspectral Mineral Identification Based on Naive Bayesian Classification Model, 34 (2014) 505-509.
[43]. Y. Ji, L. Sun, Y. Li, J. Li, S. Liu, X. Xie, Y. Xu, Non-destructive classification of defective potatoes based on hyperspectral imaging and support vector machine, Infrared Physics & Technology, 99 (2019) 71-79.
[44]. G. Ren, Y. Wang, J. Ning, Z. Zhang, Using near-infrared hyperspectral imaging with multiple decision tree methods to delineate black tea quality, Spectrochimica Acta Part A: Molecular and Biomolecular Spectroscopy, 237 (2020) 118407.
[45]. L. Pan, Q. Zhang, W. Zhang, Y. Sun, P. Hu, K. Tu, Detection of cold injury in peaches by hyperspectral reflectance imaging and artificial neural network, Food Chemistry, 192 (2016) 134-141.
[46]. R. Yuan, G. Liu, J. He, G. Wan, N. Fan, Y. Li, Y. Sun, Classification of Lingwu long jujube internal bruise over time based on visible near-infrared hyperspectral imaging combined with partial least squares-discriminant analysis, Computers and Electronics in Agriculture, 182 (2021) 106043.
[47]. C.T. Kucha, L. Liu, M.O.J.S. Ngadi, Non-Destructive Spectroscopic Techniques and Multivariate Analysis for Assessment of Fat Quality in Pork and Pork Products: A Review, 18 (2018) 377-.
[48]. H. Wang, J. Peng, C. Xie, Y. Bao, H.J.S. Yong, Fruit Quality Evaluation Using Spectroscopy Technology: A Review, 15 (2015) 11889-11927.
[49]. G. Shen, Y. Cao, X. Yin, F. Dong, J. Xu, J. Shi, Y.-W. Lee, Rapid and nondestructive quantification of deoxynivalenol in individual wheat kernels using near-infrared hyperspectral imaging and chemometrics, Food Control, 131 (2022) 108420.
[50]. P.J. Williams, P. Geladi, T.J. Britz, M.J.A.m. Manley, biotechnology, Growth characteristics of three Fusarium species evaluated by near-infrared hyperspectral imaging and multivariate image analysis, 96 (2012) 803-813.
[51]. M. Nadimi, J.M. Brown, J. Morrison, J. Paliwal, Examination of wheat kernels for the presence of Fusarium damage and mycotoxins using near-infrared hyperspectral imaging, Measurement: Food, 4 (2021) 100011.
[52]. M.A. Shahin, S.J. Symons, Detection of Fusarium damaged kernels in Canada Western Red Spring wheat using visible/near-infrared hyperspectral imaging and principal component analysis, Computers and Electronics in Agriculture, 75 (2011) 107-112.
[53]. K. Liang, J. Huang, R. He, Q. Wang, Y. Chai, M. Shen, Comparison of Vis-NIR and SWIR hyperspectral imaging for the non-destructive detection of DON levels in Fusarium head blight wheat kernels and wheat flour, Infrared Physics & Technology, 106 (2020) 103281.
[54]. R.R.P. da Conceição, M.L.F. Simeone, V.A.V. Queiroz, E.P. de Medeiros, J.B. de Araújo, W.M. Coutinho, D.D. da Silva, R. de Araújo Miguel, U.G. de Paula Lana, M.A. de Resende Stoianoff, Application of near-infrared hyperspectral (NIR) images combined with multivariate image analysis in the differentiation of two mycotoxicogenic Fusarium species associated with maize, Food Chemistry, 344 (2021) 128615.
[55]. J. Jin, L. Tang, Z. Hruska, H. Yao, Classification of toxigenic and atoxigenic strains of Aspergillus flavus with hyperspectral imaging, Computers and Electronics in Agriculture, 69 (2009) 158-164.
[56]. L.M. Kandpal, S. Lee, M.S. Kim, H. Bae, B.-K. Cho, Short wave infrared (SWIR) hyperspectral imaging technique for examination of aflatoxin B1 (AFB1) on corn kernels, Food Control, 51 (2015) 171-176.
[57]. D. Kimuli, W. Wang, K.C. Lawrence, S.-C. Yoon, X. Ni, G.W. Heitschmidt, Utilisation of visible/near-infrared hyperspectral images to classify aflatoxin B1 contaminated maize kernels, Biosystems Engineering, 166 (2018) 150-160.
[58]. F. Tao, H. Yao, Z. Hruska, R. Kincaid, K. Rajasekaran, D. Bhatnagar, A novel hyperspectral-based approach for identification of maize kernels infected with diverse Aspergillus flavus fungi, Biosystems Engineering, 200 (2020) 415-430.
[59]. H. Zhongzhi, D. Limiao, Aflatoxin contaminated degree detection by hyperspectral data using band index, Food and Chemical Toxicology, 137 (2020) 111159.
[60]. J. Gao, L. Zhao, J. Li, L. Deng, J. Ni, Z. Han, Aflatoxin rapid detection based on hyperspectral with 1D-convolution neural network in the pixel level, Food Chemistry, 360 (2021) 129968.
[61]. Q. Zhou, D. Liang, S. Fan, W. Huang, Q. Pang, X. Tian, Application of hyperspectral characteristic wavelength selection based on weighted between-class to within-class variance ratio (WBWVR) in aflatoxin B concentration classification of maize flour, Infrared Physics & Technology, 122 (2022) 104095.
[62]. G. Mishra, B.K. Panda, W.A. Ramirez, H. Jung, C.B. Singh, S.-H. Lee, I. Lee, Application of SWIR hyperspectral imaging coupled with chemometrics for rapid and non-destructive prediction of Aflatoxin B1 in single kernel almonds, LWT, 155 (2022) 112954.
[63]. X. Chu, J. Chen, Y. Tang, S. Gao, J. Zhuang, S.J.I.-P. Luo, Evaluating Growth of Colletotrichum species by Near infrared (NIR) hyperspectral imaging - ScienceDirect, 52 (2019) 257-262.
[64]. L. Yuan, P. Yan, W. Han, Y. Huang, B. Wang, J. Zhang, H. Zhang, Z. Bao, Detection of anthracnose in tea plants based on hyperspectral imaging, Computers and Electronics in Agriculture, 167 (2019) 105039.
[65]. A. Fazari, O.J. Pellicer-Valero, J. Gómez-Sanchıs, B. Bernardi, S. Cubero, S. Benalia, G. Zimbalatti, J. Blasco, Application of deep convolutional neural networks for the detection of anthracnose in olives using VIS/NIR hyperspectral images, Computers and Electronics in Agriculture, 187 (2021) 106252.
[66]. Y.-H. Yeh, W.-C. Chung, J.-Y. Liao, C.-L. Chung, Y.-F. Kuo, T.-T. Lin, Strawberry foliar anthracnose assessment by hyperspectral imaging, Computers and Electronics in Agriculture, 122 (2016) 1-9.
[67]. Y. Lu, W. Wang, M. Huang, X. Ni, X. Chu, C. Li, Evaluation and classification of five cereal fungi on culture medium using Visible/Near-Infrared (Vis/NIR) hyperspectral imaging, Infrared Physics & Technology, 105 (2020) 103206.
[68]. T. Senthilkumar, D.S. Jayas, N.D.G. White, P.G. Fields, T. Gräfenhan, Detection of fungal infection and Ochratoxin A contamination in stored barley using near-infrared hyperspectral imaging, Biosystems Engineering, 147 (2016) 162-173.
[69]. T. Senthilkumar, D.S. Jayas, N.D.G. White, Detection of different stages of fungal infection in stored canola using near-infrared hyperspectral imaging, Journal of Stored Products Research, 63 (2015) 80-88.
[70]. T. Senthilkumar, D.S. Jayas, N.D.G. White, P.G. Fields, T. Gräfenhan, Detection of fungal infection and Ochratoxin A

contamination in stored wheat using near-infrared hyperspectral imaging, Journal of Stored Products Research, 65 (2016) 30-39.
[71]. J. Farrugia, S. Griffin, V.P. Valdramidis, K. Camilleri, O. Falzon, Principal component analysis of hyperspectral data for early detection of mould in cheeselets, Current Research in Food Science, 4 (2021) 18-27.
[72]. S. Griffin, M. Magro, J. Farrugia, O. Falzon, K. Camilleri, V.P. Valdramidis, Towards the development of a sterile model cheese for assessing the potential of hyperspectral imaging as a non-destructive fungal detection method, Journal of Food Engineering, 306 (2021) 110639.
[73]. S. Ye, X. Gu, Z. Wang, Y. Huang, L.J.F.S. Pan, Growth Simulation and Discrimination of Botrytis cinerea, Rhizopus stolonifer and Colletotrichum acutatum Using Hyperspectral Reflectance Imaging, 10 (2015) e0143400.
[74]. H. Jiang, X. Jiang, Y. Ru, Q. Chen, X. Li, L. Xu, H. Zhou, M. Shi, Rapid and non-destructive detection of natural mildew degree of postharvest Camellia oleifera fruit based on hyperspectral imaging, Infrared Physics & Technology, 123 (2022) 104169.
[75]. Y.R. Zhao, K.Q. Yu, X. Li, Y.J.S.R. He, Detection of Fungus Infection on Petals of Rapeseed (Brassica napus L.) Using NIR Hyperspectral Imaging, 6 (2016) 38878.
[76]. P. Williams, T.L. Kammies, P. Gouws, M.J.J.o.S.I. Manley, Effect of colony age on near infrared hyperspectral images of foodborne bacteria, 8 (2019).
[77]. Lin, Huang, Jiewen, Zhao, Quansheng, Chen, Yanhua, Z.J.F.R. International, Rapid detection of total viable count (TVC) in pork meat by hyperspectral imaging, (2013).
[78]. Y.Z. Feng, D.W.J.T. Sun, Determination of total viable count (TVC) in chicken breast fillets by near-infrared hyperspectral imaging and spectroscopic transforms, 105 (2013) 244-249.
[79]. D. Li, F. Zhang, J. Yu, X. Chen, B. Liu, X. Meng, A rapid and non-destructive detection of Escherichia coli on the surface of fresh-cut potato slices and application using hyperspectral imaging, Postharvest Biology and Technology, 171 (2021) 111352.
[80]. F. Tao, Y. Peng, Y. Li, K. Chao, S. Dhakal, Simultaneous determination of tenderness and Escherichia coli contamination of pork using hyperspectral scattering technique, Meat Science, 90 (2012) 851-857.
[81]. Y.-Z. Feng, W. Yu, W. Chen, K.-K. Peng, G.-F. Jia, Invasive weed optimization for optimizing one-agar-for-all classification of bacterial colonies based on hyperspectral imaging, Sensors and Actuators B: Chemical, 269 (2018) 264-270.
[82]. E. Bonah, X. Huang, J.H. Aheto, R. Yi, S. Yu, H. Tu, Comparison of variable selection algorithms on vis-NIR hyperspectral imaging spectra for quantitative monitoring and visualization of bacterial foodborne pathogens in fresh pork muscles, Infrared Physics & Technology, 107 (2020) 103327.
[83]. Q. Gu, L. Sheng, T. Zhang, Y. Lu, Z. Zhang, K. Zheng, H. Hu, H. Zhou, Early detection of tomato spotted wilt virus infection in tobacco using the hyperspectral imaging technique and machine learning algorithms, Computers and Electronics in Agriculture, 167 (2019) 105066.
[84]. H. Lee, M.S. Kim, H.-S. Lim, E. Park, W.-H. Lee, B.-K. Cho, Detection of cucumber green mottle mosaic virus-infected watermelon seeds using a near-infrared (NIR) hyperspectral imaging system: Application to seeds of the "Sambok Honey" cultivar, Biosystems Engineering, 148 (2016) 138-147.

Table 1 Development of various microorganisms in the detection of hyperspectral techniques.

Detection object	product	Spectral range	Wavelengths selection methods	The modeling method	Accuracy	reference
F.Subglutinans F.Proliferatum F.Verticillioides	NA	1100-2200nm	PCA	PLS-DA	98.6%;66.6%;16.8%	[25]
Fusarium;DON	Wheat	960nm-1700nm	All band	1-KNN 3-KNN	FDK 85%、DON 80%	[51]
DON	Wheat	900nm-1700nm	All band	PLS;SVM;LPLS-S	RMSEC = 47.37mg/kg;42.39mg/kg; 40.25mg/kg RPD = 1.92;2.04;2.24	[49]
Fusarium	Wheat	400-1000 mm	All band	LDA	92%	[52]
Fusarium DON	Wheat	400 -1000 nm 1000-2500nm	GA	MSC-GA-SAE;SNV-GA-SAE	100%;96%	[53]
F.verticillioides、F.graminearum	Maize	1000-2062nm	PCA	PLS-DA	100%	[54]
AF38;F283; AF2038		400-1000 nm	GA	SVM	75%;97%;99%	[55]
AFB_1	Maize (yellow, white, purple)	1100-1700mm		PLS-DA	90.7%;92.3%; 96.9%	[56]
AFB1	Maize	400-1000 nm	PCA	FDA	>96%	[57]
AFB1	Maize	1000-2500nm	PCA	FDA、PLS-DA	100%;96%	[57]
AF13、AF36	Maize	900-2500 nm	RF	PLS-DA I-RF-PLSDA; II-RF-PLSDA	96.3%;97.8%	[58]
AFB1	Peanut,	400-1000 nm	RBF	RBF-SVM	95.5% RMSE = 0.0223 R^2 = 0.9785	[59]
AFB1	Maize、Peanut	400-1000 nm		1D-CNN	92.11%;96.35%; 94.64%	[60]
AFB	maize flour.	430-1000 nm; 1000-2400nm	BWVR; WBWVR	SVM;KNN; DT	96.18%	[61]
AFB1	Almond kernels	900-1700 nm	CARS	PLSR	R_2 = 0.958 RMSEP=0.089ug/g	[62]
Colletatrichmtrsrcanm;Colexotrichwmpgloeoxponioidex	potato	400-1000 nm	CARS	PCA;SVM	90.83%;94.17%	[63]
Gloeosporiumtheae-sinesis Miyake	tea leaf	450-950nm	SectralRtioAalysis；AN Independent T-Text	TARI；TANI.	98%；94%	[64]
Anthracnose	olive	450-1050 nm		DL-CNN	>85%	[65]
Anthracnose	Strawberry foliar	450-950	PLS	SAM;SDA; CM	80%;82%;94%	[66]
Aspergillus parasiticus, Aspergillus flflavus, Aspergillus glaucus, Aspergillus niger and Penicillium sp.,		400-1000 nm	SPA	SVM	91.26%;87.30%;97.62%; 99.20%;91.27%	[67]
Aspergillus glaucus ;Penicilliumspp	Canola	1000-1600nm	PCA	LDA;QDA	>90%	[68]
Aspergillus glaucus ;Penicilliumspp; Ochratoxin A	Barley	1000-1600nm	PCA	linear, quadratic, and Mahalanobis statistical classifiers	>94%;82%	[69]
Aspergillus glaucus ;Penicilliumspp; Ochratoxin A	wheat	1000-1600nm	PCA	linear, quadratic, and Mahalanobis statistical classifiers	>90%;>98%	[70]

sporulation	cheeseslets	400-1000 nm		PCA	>99%	[71]
Botrytis cinereal; Rhizopus stolonifera; Colletotrichum acutatum	Peach	400-1000 nm	PCA	PLSDA	R^2 = 0.9292;0.9927;0.7382;0.8594 97.5%	[73]
Sclerotinia sclerotiorum	Brassica napus	874-1734 nm	PCA;RF	LS-SVM	97.48%	[75]
natural mildew	Camellia oleifera	400-1000 nm	2DCOS; SPA; CARS	PLSDA; KNN; CART	90.8%;83.3%	[74]
Bacillus; Escherichia coli; Staphylococcus aureus; Staphylococcus; epidermidis		920-2514 nm	PCA	PLSDA;	82.0 ~ 99.96%	[76]
TVC	prok	450-900 nm	PCA;PLS	BP-ANN	RMSEP = 0.243 lg CFU/g; R_p^2 = 0.8308	[77]
TVC	chicken breast	900-1700 nm	AF;AS; K-M	PLSR	R=0.96 $RMSEP_s$ = 0.4 lg CFU/g	[78]
Escherichia coli	Potato	400-1000 nm	GA	BP-NN; PLS	R^2 = 0.976; 0.891	[79]
Escherichia coli	Pork	400-1100 nm		MLR	R_{cv} =0.877; 0.841	[80]
Escherichia coli O8, O11,O138; Listeria monocytogens; Listeria seeligeri; Staphyloccocus aureus	agar plate	400-1050 nm	CARS; GA; SPA	PLSDA; SVM	97.0%; 96.0%	[81]
Escherichia coli O157 ; Staphylococcus aureus	Pork	400-1000 nm	MPA; Intelligent Optimization Algorithms; HVSM;CARS; VCPA;MPA	PLS	R^2_p = 0.9977,0.9960; RMSEP = 0.1532,0.1225; RPD = 13.59,16.8032	[82]
Wilt virus	tobacco	400-1000 nm	SPA;BRT;GA	BRT; SVM; RF;CART	85.2%;77.6% 81.9%;72.4% 72.4%;	[83]
CGMMV	watermelon seeds	948-2046 nm		PLS-DA; LS-SVM	94.7%;94.7%	[84]

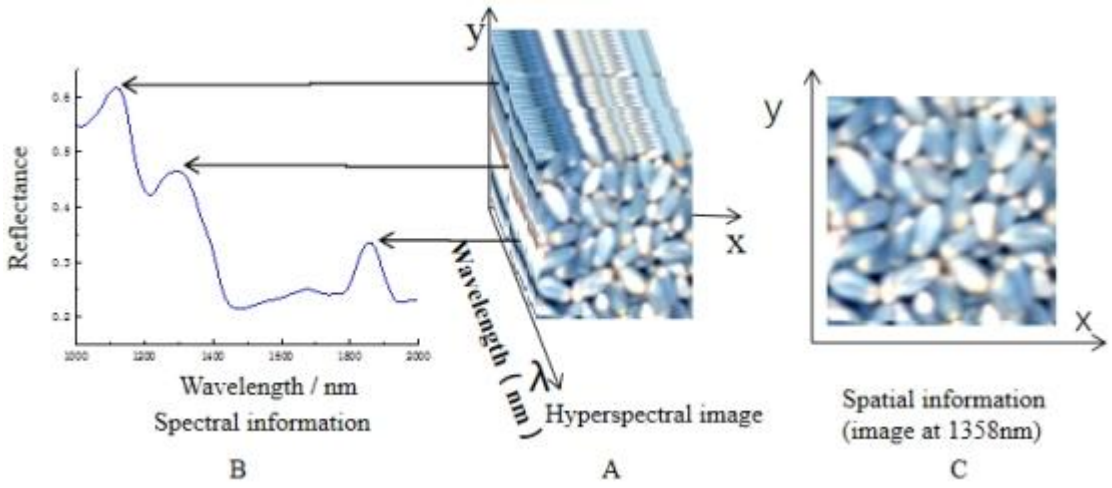

Figure 1. Wheat kernel kernel hypercube prepared by HSI technology

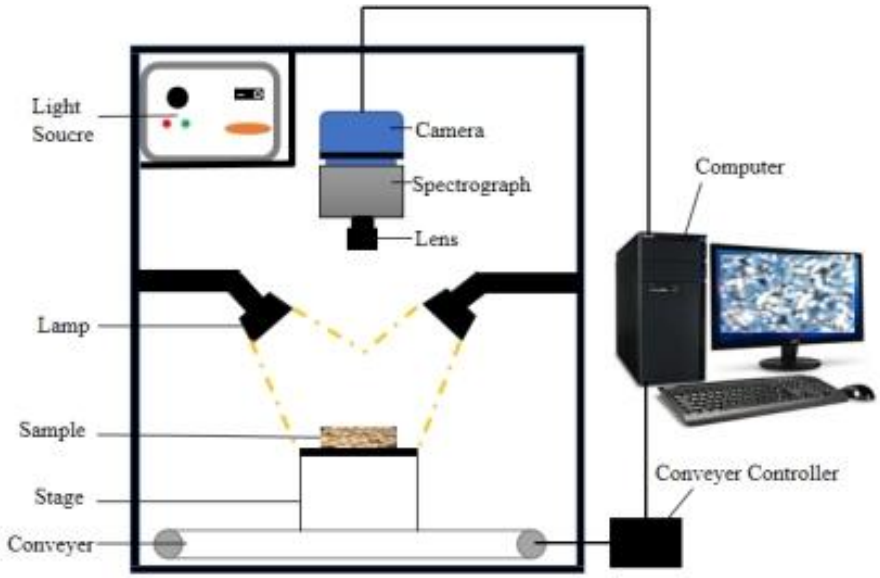

Figure 2. A classical HSI system

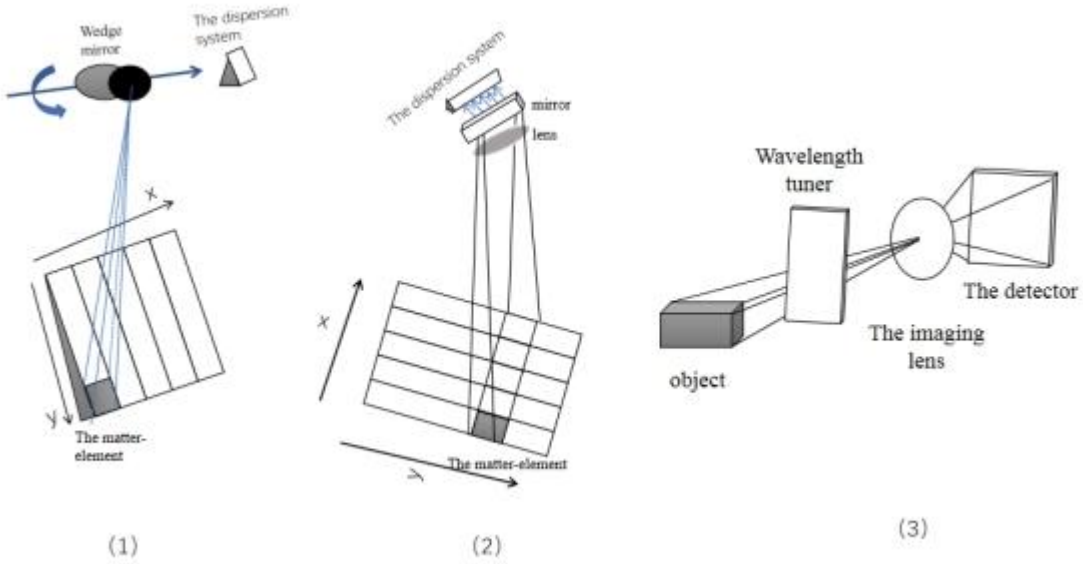

Figure 3.Three acquisition modes of hyperspectral images

Professor Lianming Xia, et. al. "Application of Hyperspectral Imaging Technology for Microbial Contamination Detection: A Review." *IOSR Journal of Agriculture and Veterinary Science (IOSR-JAVS)*, 16(3), 2023, pp. 01-16.